Research Square

Preprints are preliminary reports that have not undergone peer review.
They should not be considered conclusive, used to inform clinical practice,
or referenced by the media as validated information.

Complex Network Analysis of Temperature Variability in Semi-Arid Central Tanzania Using Visibility Graphs

SHABAN ALLY

sshabyjally@gmail.com

Andhra University https://orcid.org/0009-0008-2859-6922

B. MUNISWAMY

Andhra University https://orcid.org/0000-0003-4277-9502

B. Punyavathi

Andhra University

Research Article

Keywords:

Posted Date: November 24th, 2026

DOI: https://doi.org/10.21203/rs.3.rs-11836713/v1

License: This work is licensed under a Creative Commons Attribution 4.0 International License.
Read Full License

Additional Declarations: The authors declare no competing interests.

Complex Network Analysis of Temperature Variability in Semi-Arid Central Tanzania Using Visibility Graphs

Shaban Juma Ally[a,b,*], Begari Muniswamy[a], B. Punyavathi[a]

[a]*Department of Statistics, Andhra University, Visakhapatnam 530003, Andhra Pradesh, India*
[b]*College of African Wildlife Management, Mweka, P.O. Box 3031, Moshi, Kilimanjaro, Tanzania*

Abstract

Most existing studies on the features of temperature in semi-arid central Tanzania have focused on linear trends and other statistical properties, while the internal dynamics of temperature variability remain largely unknown. The visibility graph algorithm transforms a time series into a complex network whose structure reflects the dynamics of the series. In this study, the algorithm is applied to the monthly maximum, minimum and mid-range temperatures of Dodoma, Singida and Tabora for 1981–2024, and the resulting networks are characterised by their node degrees, degree distributions and triadic motifs, complemented by persistence exponents and annual and seasonal trend tests. The main characteristics obtained are as follows: the 1998–1999 hot season forms a hub of the temperature networks in all three regions; the most connected months all fall in the October–March hot season, so the annual cycle organises the networks; the ordering of successive months changed around 2000, when minimum temperature shifted upwards; minimum temperature warmed significantly until 2014 (0.18–0.24 °C per decade, $p \leq 0.014$), whereas maximum temperature fell abruptly after 2015; and, by season, maximum temperature decreased during the March–May rains while the dry season warmed, so that the temperature range narrowed in most seasons. Visibility-graph measures therefore show the seasonal organisation and regime changes of temperature variability that trend analysis alone does not reveal.

Keywords: Visibility graph, Complex network, Temperature variability, Network motifs, Temperature range, Hurst exponent, Central Tanzania

1. Introduction

Rising concentrations of greenhouse gases have warmed the Earth's surface by about 1.1 °C since the late nineteenth century [1], and the resulting changes in heat extremes, evaporative demand and water availability are felt most acutely in drylands where farming depends on rainfall. In East Africa, year-to-year climate is additionally shaped by sea-surface temperature patterns in the Pacific and Indian Oceans, most notably the El Niño–Southern Oscillation (ENSO) and the Indian Ocean Dipole (IOD) [2, 3]. Downscaled projections for Tanzania point to further warming during the present century under both intermediate and high emission scenarios [4, 5].

*Corresponding author.
Email address: sshabyjally@gmail.com
Preprint submitted to Communications in Nonlinear Science and Numerical Simulation

Dodoma, Singida and Tabora lie on the largely semi-arid central plateau of Tanzania, which receives a single rainy season followed by a long, hot and dry period. Crop and livestock production there are sensitive to heat stress, so knowing how temperature varies is of direct practical value. Existing work on the area is largely trend-based. Using station archives for 1961–2013, Myeya [6] detected significant warming of both minimum and maximum temperature in Dodoma Region with the Mann–Kendall test, and Msilu et al. [7] reported rising temperatures together with irregular rainfall in the Bahi and Mpwapwa districts over 1981–2021. Such analyses quantify the direction and rate of change but treat a series as a trend plus random noise. They do not reveal whether warm months cluster in time, which months shape the record most, or whether the way successive months follow one another has changed.

Answering those questions requires tools that describe the ordering of observations, not only their distribution, and complex-network representations of time series provide such tools. A series can be mapped onto a graph in several ways — for instance by linking cycles of a pseudo-periodic signal [8] or recurrent states in phase space [9] — after which standard graph measures summarise its structure. The visibility graph (VG) [10] is attractive because it requires no embedding parameters: each observation becomes a node, and two nodes are joined when the straight line between their values passes above all intermediate values. The topology of the graph reflects the process that generated the series: periodic series map onto regular graphs [10]; in the horizontal variant of the algorithm, every uncorrelated series produces the same exponentially decaying degree distribution [11]; and fractal processes produce power-law tails in the natural visibility graph, with an exponent linked to the Hurst exponent [12, 13]. Small subgraphs, or motifs, give a finer description of local ordering [14–16].

Network approaches are now well established in climate research [17, 18]. Visibility graphs in particular have been used to flag unusual hurricane seasons in the United States [19], to analyse temperature series from Yucatán [20], to examine air-temperature anomalies [21], and to characterise temperature in Xi'an [22] and precipitation in Shanghai [23]. Cao et al. [23] showed that combining degree, motif and degree-distribution analyses with moving windows can isolate the few extreme events that dominate a climate record. We are not aware of any visibility-graph study of temperature in semi-arid East Africa.

This study addresses that gap. Forty-four years of monthly maximum and minimum temperature for the three regions are mapped onto visibility graphs directly, keeping the annual cycle that dominates the local thermal regime, and three questions are examined: which months exert the greatest influence on the network, and how does this depend on season and on temperature itself; has the local ordering of successive months, measured by triadic motifs, changed over time; and what do the degree distributions and the persistence of the series reveal about the underlying dynamics.

2. Data and methods

2.1. Study area and data

The study was conducted in Dodoma, Singida, and Tabora regions of semi-arid central Tanzania, characterised by a unimodal rainfall regime extending from November/ December to April. Monthly maximum ($T_{\max}$) and minimum ($T_{\min}$) air temperatures at 2 m above the surface were obtained from the NASA Prediction of Worldwide Energy Resources (NASA POWER) database [24] for the period 1981–2024. The dataset comprised

528 consecutive monthly observations per region for each temperature variable, with no missing values, ensuring temporal continuity for statistical analysis. Validation against ground-based meteorological observations indicated strong agreement, with correlation coefficients exceeding 0.90.

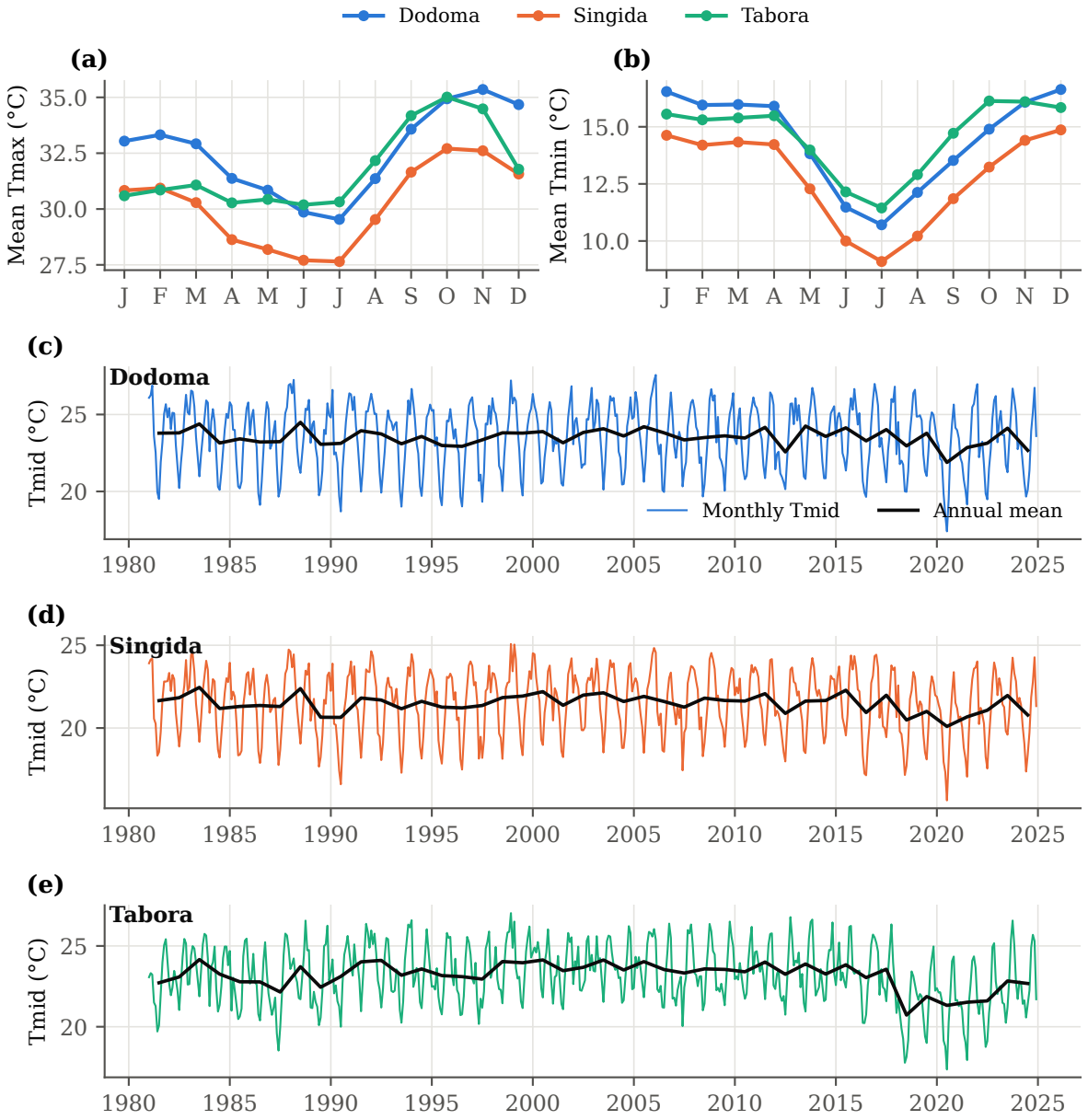

Figure 1: Temperature in the study area, 1981–2024. (a) Mean annual cycle of $T_{\max}$ and (b) of $T_{\min}$. (c)–(e) Monthly mid-range temperature T_{mid} in Dodoma, Singida and Tabora (coloured lines) with annual means (black lines).

2.2. Visibility graph

Let $\{x_i\}$, $i = 1, \ldots, N$, be one of the temperature series of a region (Fig. 1): $T_{\max}$, $T_{\min}$ or the mid-range temperature $T_{\mathrm{mid}} = (T_{\max} + T_{\min})/2$. T_{mid}, which combines both variables, is the main series of the network analysis, and the degree, degree-distribution

and persistence measures are repeated for $T_{\max}$ and $T_{\min}$. Here x_i is the temperature (°C) of month i and t_i its time index; for the full record $N = 528$, and the annual cycle is not removed. Every month is a node. Two months a and b ($t_a < t_b$) are linked if no intermediate month c reaches the straight segment joining (t_a, x_a) and (t_b, x_b), that is, if

$$x_c < x_a + (x_b - x_a)\,\frac{t_c - t_a}{t_b - t_a}, \qquad t_a < t_c < t_b \tag{1}$$

holds for every c between them; consecutive months are therefore always linked [10]. Collecting all links gives a symmetric adjacency matrix $\mathbf{A}$, with $A_{ij} = 1$ when i and j are linked and 0 otherwise, and the degree of month i is

$$k_i = \sum_{j=1}^{N} A_{ij} \tag{2}$$

Fig. 2 applies the construction to the Dodoma T_{mid} series of 2015–2016. Because each node sees at least its immediate neighbours, the graph is always connected, and its links carry no direction. Expressing the temperatures in another unit (an affine transformation), or adding a linear trend, leaves every link unchanged; the latter follows from Eq. (1), because a term proportional to time raises both sides of the inequality by the same amount. The degree of a month measures how far along the record its value can be "seen". Because the annual cycle is retained, the hot months of each year stand above the cool-season trough and can see across it to other hot seasons, whereas mid-year months lie in the trough and mainly see their neighbours. Within a given season, a month gains links when it exceeds the corresponding months of neighbouring years. Degree is therefore interpreted here as the prominence of a month within the thermal history, combining its seasonal position with how unusual it is, and the degree distribution $P(k)$ — the fraction of months with degree k — as the distribution of that prominence. The meaning of a hub depends on the variable. In a $T_{\max}$ network, a high-degree month is one whose maximum temperature rose above those of the surrounding months and years; in a $T_{\min}$ network, it is a month whose minimum temperature stayed unusually high; and in a T_{mid} network, it is a month whose whole thermal range was displaced upwards. Because the visibility criterion favours large values, unusually cold months appear in these networks as months of low degree rather than as hubs.

2.3. Triadic time-series motifs

Motifs — small subgraphs that occur more or less often than expected by chance — summarise the local wiring of a network [25]. In visibility graphs, motifs defined on temporally ordered nodes describe how successive values relate to one another [14–16]. Following the triadic scheme adapted to natural visibility graphs by Cao et al. [23], we consider triplets of months $i < j < k$ in which i sees j and j sees k horizontally, i.e. every value lying between them is lower than both end points:

$$x_i, x_j > x_n \quad \forall n \in (i, j) \qquad \text{and} \qquad x_j, x_k > x_m \quad \forall m \in (j, k) \tag{3}$$

Each such triplet is classified by the rank order of its three values (1 = lowest, 3 = highest). The six possible orders (1, 2, 3), (1, 3, 2), (2, 1, 3), (2, 3, 1), (3, 1, 2) and (3, 2, 1) are labelled M_1 to M_6. When the middle value is the smallest (M_3, M_5), the two outer months always see each other and the triad is closed; when it is the largest

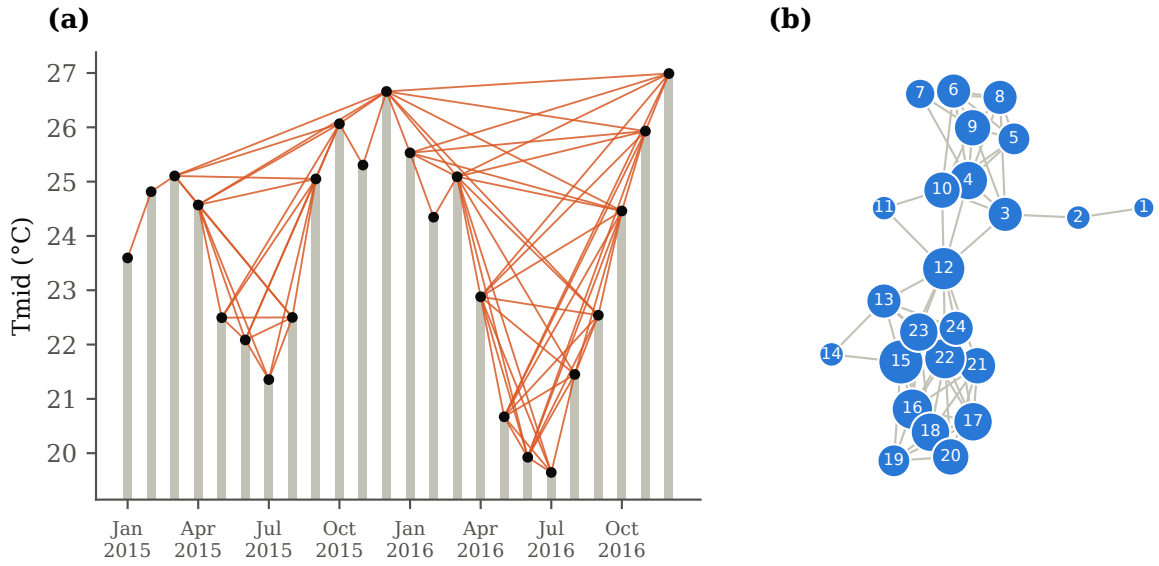

Figure 2: Construction of a visibility graph from the Dodoma T_{mid} series, January 2015 – December 2016. (a) Monthly values with all visibility links drawn in orange. (b) The same graph drawn as a network; labels give the month number (1 = January 2015) and node area increases with degree.

(M_2, M_4), they cannot see each other and the triad is open. For the monotonic orders, closure depends on curvature: a rising or falling triplet whose middle value lies below the chord joining the outer values satisfies Eq. (1) and is closed. These closed monotonic forms are labelled M_7 (rising) and M_8 (falling), and M_1 and M_6 are kept for the open forms, giving the eight motifs of Fig. 3. In a temperature series each motif has a direct reading: in M_2 and M_4 the middle month is the warmest of the three (a warm peak); in M_3 and M_5 it is the coolest (a cool dip); M_1 and M_7 are warming sequences and M_6 and M_8 cooling sequences, closed when the middle month lies below the chord. A smooth seasonal oscillation produces long monotonic runs and regular troughs, so a record dominated by its annual cycle is expected to depart strongly from the white-noise profile, whereas irregular month-to-month fluctuations favour isolated peaks and dips. Motifs were counted in the T_{mid} series. The relative frequency of motif q within a window is

$$f_q = \frac{N_q}{\sum_{q'=1}^{8} N_{q'}}, \qquad q = 1, 2, \ldots, 8 \tag{4}$$

where N_q is the number of occurrences of motif q. As a reference, motifs were counted in 20 Gaussian white-noise series of 2000 points each, giving the uncorrelated profile f_0 = (0.135, 0.199, 0.100, 0.200, 0.102, 0.136, 0.064, 0.064). The pooled frequencies of M_1 + M_7 and M_6 + M_8 (0.199 and 0.200) and those of M_2–M_5 (0.199, 0.100, 0.200 and 0.102) match the theoretical horizontal-visibility values for random series [16, 23].

To follow how the motif profile of T_{mid} evolves, frequencies were computed in moving windows and standardised across windows,

$$\zeta_q(t) = \frac{f_q(t) - \langle f_q \rangle}{\sigma_{f_q}} \tag{5}$$

where $\langle f_q \rangle$ and σ_{fq} are the mean and standard deviation of f_q over all windows. The eight-element vectors $\zeta(t_i)$ and $\zeta(t_j)$ were then correlated for every pair of windows to

give a similarity coefficient $s(t_i, t_j)$; a high value indicates that two periods share a similar local arrangement of successive months, that is, similar proportions of warm peaks, cool dips and warming or cooling sequences.

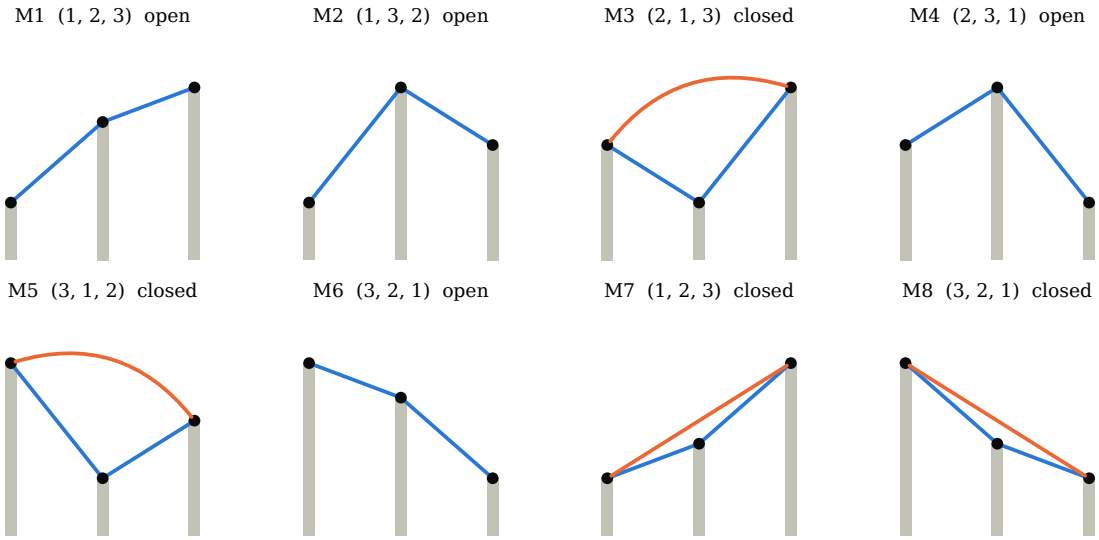

Figure 3: The eight triadic motifs used in this study. Grey bars are the three data values, blue segments the visibility links required by Eq. (3), and an orange segment a link between the outer values, which makes the triad closed (M_3, M_5, M_7, M_8).

2.4. Moving windows, degree distribution, persistence and trends

Moving windows. Whether a month is a hub depends on the period against which it is compared: a month may dominate a decade yet be ordinary within the full record. To test this, windows of $W = 5, 10, \ldots, 40$ years were advanced through the 44-year T_{mid} series in steps of $s = 1$ year (Fig. 4), giving

$$n = \frac{44 - W}{s} + 1 \tag{6}$$

windows for each W (from 40 windows at $W = 5$ to 5 windows at $W = 40$). A separate visibility graph was built for every window, and the degree of each month and the correlation between temperature and degree were recomputed within it. Motif profiles of T_{mid} were computed in 120-month (10-year) windows advanced by one month, giving 409 windows per region.

Degree distribution. Because the annual cycle gives most months a moderate number of links, $P(k)$ of a temperature network rises to a maximum at the modal degree k_{mode} before it decays: months confined to the cool-season trough supply the low degrees, and hot-season months that stand above their surroundings populate the tail. The tail ($k \geq k_{\mathrm{mode}}$) of the T_{mid}, T_{max} and T_{min} distributions was therefore fitted with

$$P\,(k) = c \cdot k^{-\gamma} \tag{7}$$

by ordinary least squares on logarithmic axes, and fit quality was summarised by the adjusted R^2. Because log–log regression can be biased [26], γ was also estimated with the discrete maximum-likelihood approximation given in that study. The power law was

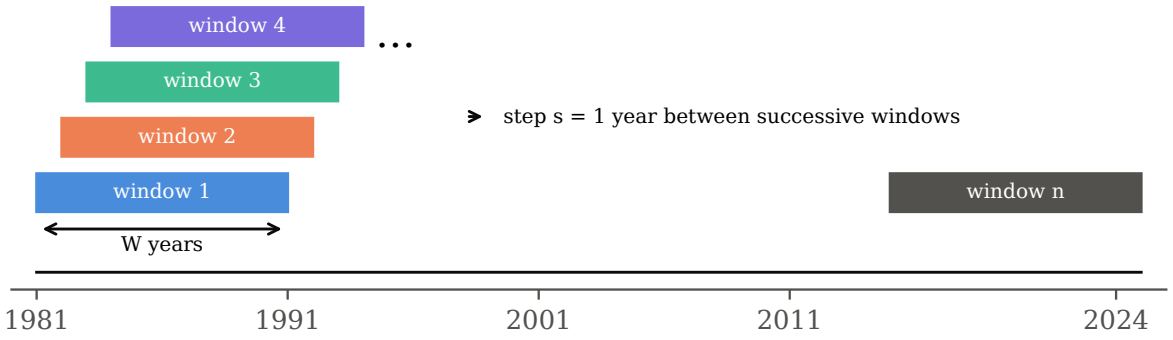

Figure 4: Scheme of the moving-window procedure: windows of W years advance by one year, and a separate visibility graph is constructed in each.

compared with an exponential decay $P(k) \propto e^{-\lambda k}$ fitted over the same range, which is the exact form for uncorrelated series in the horizontal visibility graph [11]. A power-law tail implies a network containing a few highly connected hubs [27]; for a temperature record, it means that a small number of months dominate the visibility structure of the whole series.

Persistence. The Hurst exponent H of the monthly T_{mid}, $T_{\max}$ and $T_{\min}$ series was estimated by rescaled-range (R/S) analysis [28] from the scaling relation

$$E\left[\frac{R(n)}{S(n)}\right] = C \cdot n^{H} \tag{8}$$

where $R(n)$ is the range of cumulative departures from the mean and $S(n)$ the standard deviation of sub-series of length n. $H \approx 0.5$ characterises an uncorrelated series, $H > 0.5$ a persistent series and $H < 0.5$ an anti-persistent, mean-reverting series. For temperature, $H > 0.5$ means that warm (cool) months tend to be followed by further warm (cool) months, whereas $H < 0.5$ means that warm and cool departures tend to alternate. The detrended fluctuation analysis (DFA) exponent α [29] of T_{mid} was computed as an independent estimate. Because the series retain the annual cycle, both exponents describe the combined effect of the seasonal oscillation and of year-to-year variability.

Trends and abrupt changes. Annual and seasonal means of $T_{\max}$, $T_{\min}$, T_{mid} and the temperature range $\mathrm{TR} = T_{\max} - T_{\min}$, whose narrowing indicates asymmetric warming [30], were tested for monotonic trends with the Mann–Kendall statistic [31, 32]

$$S = \sum_{i=1}^{n-1} \sum_{j=i+1}^{n} \operatorname{sgn}\left(x_j - x_i\right) \tag{9}$$

whose variance, for n independent and randomly ordered values without ties, is

$$\operatorname{Var}(S) = \frac{n\,(n-1)\,(2n+5)}{18} \tag{10}$$

Positive autocorrelation inflates the significance of S, so the variance was also corrected following Hamed and Rao [33], using the autocorrelation ρ_k^R of the ranks of the detrended series at those lags k where it is significant at the 5% level:

$$\frac{n}{n^*} = 1 + \frac{2}{n\,(n-1)\,(n-2)} \sum_{k=1}^{n-1} (n-k)\,(n-k-1)\,(n-k-2)\,\rho_k^R \tag{11}$$

The standardised test statistic is

$$Z_{\mathrm{MK}} = \frac{S - \operatorname{sgn}(S)}{\sqrt{\operatorname{Var}(S) \cdot \frac{n}{n^*}}} \tag{12}$$

with $n/n^* = 1$ for the original test. Trend magnitude was estimated with the Sen slope [34],

$$\beta = \operatorname{median}\left(\frac{x_j - x_i}{j - i}\right), \qquad 1 \le i < j \le n \tag{13}$$

Seasonal means were formed for December–February (DJF, rainy season), March–May (MAM, end of the rains), June–August (JJA, cool dry season) and September–November (SON, hot dry season); each DJF season is assigned to the year of its January and February, so the incomplete DJF of 1981 is excluded (43 DJF and 44 other seasonal values). The seasonal analysis involves 48 tests per period (3 regions × 4 seasons × 4 variables), so its p-values were adjusted for multiple testing with the Benjamini–Hochberg false-discovery-rate procedure [35], and a seasonal trend is called significant when the adjusted value $q < 0.05$. In one case (Singida, DJF $T_{\max}$, 1981–2014) the estimated correction factor n/n^* was not positive, and the uncorrected variance was used. Because the results revealed an abrupt change in 2015–2016 (Section 3.1), all trends were computed both for 1981–2024 and for 1981–2014. The timing of abrupt shifts in the annual means of the four variables was located with the Pettitt test [36], whose statistic and approximate significance level are

$$U_t = \sum_{i=1}^{t} \sum_{j=t+1}^{N} \operatorname{sgn}(x_i - x_j) \tag{14}$$

$$K = \max_{1 \le t < N} |U_t| \tag{15}$$

$$p \approx 2 \exp\left(\frac{-6K^2}{N^3 + N^2}\right) \tag{16}$$

where the change point is the year t at which $|U_t|$ reaches its maximum K.

Surrogate test. The T_{mid}, $T_{\max}$ and $T_{\min}$ series of each region were randomly reordered 100 times and all network measures were recomputed. Shuffling keeps the set of temperatures, and hence their mean, variance and distribution, but destroys their order in time, including the annual cycle and any persistence. Properties that survive shuffling therefore stem from the distribution of temperatures, whereas properties that change depend on the sequence in which the temperatures occur.

3. Results and discussion

3.1. Temperature trends and change points

Table 1 summarises the trends. Over 1981–2014, $T_{\min}$ rose significantly in all three regions, by 0.216 °C per decade in Dodoma ($p = 0.010$), 0.179 °C per decade in Singida ($p = 0.014$) and 0.237 °C per decade in Tabora ($p = 0.005$), whereas $T_{\max}$ showed no significant trend (−0.105, −0.053 and +0.168 °C per decade; $p \ge 0.17$). The temperature range therefore narrowed significantly in Dodoma (−0.351 °C per decade) and Singida (−0.216 °C per decade) but not in Tabora, and T_{mid}, which averages the two, showed no significant trend in any region.

Table 1: Mean values and trends of annual temperature in the three regions.

Region	Var.	Mean ± SD (°C)	Sen slope 1981–2024 (°C/decade)	MK p	Modified MK p	Sen slope 1981–2014 (°C/decade)	Modified MK p (1981–2014)
Dodoma	T_{mid}	23.52 ± 2.06	−0.052	0.578	0.484	+0.058	0.495
	T_{max}	32.57 ± 2.44	−0.267	0.012	0.012	−0.105	0.358
	T_{min}	14.47 ± 2.21	+0.188	0.001	0.001	+0.216	0.010
	TR	18.10 ± 2.17	−0.454	< 0.001	< 0.001	−0.351	< 0.001
Singida	T_{mid}	21.48 ± 1.91	−0.073	0.327	0.327	+0.058	0.495
	T_{max}	30.19 ± 2.29	−0.282	0.010	0.010	−0.053	0.594
	T_{min}	12.78 ± 2.14	+0.151	0.002	0.002	+0.179	0.014
	TR	17.41 ± 2.26	−0.437	< 0.001	< 0.001	−0.216	0.035
Tabora	T_{mid}	23.18 ± 1.80	−0.107	0.245	0.441	+0.170	0.080
	T_{max}	31.78 ± 2.49	−0.288	0.077	0.267	+0.168	0.173
	T_{min}	14.58 ± 1.79	+0.074	0.288	0.288	+0.237	0.005
	TR	17.20 ± 2.42	−0.374	< 0.001	0.059	−0.046	0.678

Note: mean ± SD of the monthly values; trends computed on annual means. T_{max} and T_{min} are the monthly maximum and minimum temperature, $T_{\mathrm{mid}} = (T_{\mathrm{max}} + T_{\mathrm{min}})/2$ and $\mathrm{TR} = T_{\mathrm{max}} - T_{\mathrm{min}}$. MK = Mann–Kendall test; modified MK = variance corrected for serial correlation [33].

The picture changes after 2015. T_{max} dropped abruptly in all three regions, so that its 2016–2024 mean is 1.0 °C (Dodoma), 1.3 °C (Singida) and 2.4 °C (Tabora) lower than its 2005–2014 mean; in Tabora, T_{min} also fell, by 0.6 °C. Over the full period this step produces negative T_{max} trends of 0.267–0.288 °C per decade, significant in Dodoma and Singida ($p \approx 0.01$) but not in Tabora ($p = 0.077$, or 0.27 after correction for serial correlation), and it reverses the sign of the Tabora T_{mid} trend. TR decreased over 1981–2024 by 0.37–0.45 °C per decade, significantly in Dodoma and Singida under both tests and in Tabora only under the original test ($p < 0.001$, compared with 0.06 after correction). Full-period T_{min} trends remain significant in Dodoma and Singida (0.188 and 0.151 °C per decade) but not in Tabora, where the post-2015 decrease offsets the earlier warming.

The Pettitt test on the annual means (Table 2) places an upward shift in T_{min} after 1999 in Dodoma ($p < 0.001$) and after 1999 in Singida ($p = 0.003$), with annual means 0.55 and 0.41 °C higher afterwards; the shift in Tabora (after 1997) is not significant. T_{max} shifts downwards after 2011 in Singida ($p = 0.037$) and after 2013 in Tabora ($p = 0.011$), and TR decreases significantly in all three regions, after 2000 (Dodoma), 2005 (Singida) and 2013 (Tabora). A step of 1.0–2.4 °C occurring almost simultaneously in three neighbouring regions may be a genuine regional change — the persistent cool period of 2018–2022 is clearly visible in Fig. 1(c–e), and the lowest monthly T_{mid} of every region occurred in 2020 (Table 2). However, gridded reanalysis records can also contain artificial jumps when the observations assimilated by the model change [37], so their homogeneity is not guaranteed. Although the series correlate closely with station observations (Section 2.1), a high correlation does not exclude a shift in level, so the magnitude of the post-2015 step should be confirmed with station records before it is interpreted climatically. The warming of T_{min} agrees with the night-time warming reported for Dodoma station records by Myeya [6], whereas the significant warming of maximum temperature reported in that study for 1961–2013 is not seen in the monthly maxima analysed here for 1981–2014; the difference may reflect the different periods and data sources (station observations versus gridded reanalysis).

Table 3 breaks the trends down by season. Over 1981–2024, TR decreased in all twelve region–season combinations, by 0.14–0.92 °C per decade, and the decrease is significant

Table 2: Record monthly values and Pettitt change points of the annual means.

Region	Var.	Highest monthly value (°C)	Lowest monthly value (°C)	Pettitt break	Annual mean before → after (°C)	Pettitt p
Dodoma	T_{mid}	27.57 (Feb 2006)	17.41 (Jul 2020)	2017	23.61 → 23.06	0.570
	T_{max}	37.05 (Oct 2023)	25.99 (Jun 2020)	2006	32.88 → 32.11	0.114
	T_{min}	18.26 (Feb 2006)	8.73 (Jul 2020)	1999	14.16 → 14.71	< 0.001
	TR	22.73 (Sep 1996)	10.07 (Jan 2024)	2000	18.71 → 17.58	< 0.001
Singida	T_{mid}	25.07 (Dec 1998)	15.63 (Jul 2020)	2015	21.61 → 21.00	0.231
	T_{max}	35.46 (Feb 1999)	24.00 (Jun 2020)	2011	30.52 → 29.40	0.037
	T_{min}	16.10 (Feb 2024)	7.02 (Jul 2020)	1999	12.54 → 12.96	0.003
	TR	21.94 (Sep 1996)	10.58 (Apr 2016)	2005	17.91 → 16.76	< 0.001
Tabora	T_{mid}	27.03 (Dec 1998)	17.36 (Jul 2020)	2015	23.45 → 22.13	0.028
	T_{max}	36.71 (Feb 1999)	25.71 (Jun 2018)	2013	32.26 → 30.33	0.011
	T_{min}	18.20 (Dec 1998)	8.40 (Jul 2020)	1997	14.41 → 14.69	0.220
	TR	21.48 (Aug 1992)	10.54 (Jan 2018)	2013	17.63 → 15.89	< 0.001

Note: the break year is the last year before the shift.

Table 3: Seasonal trends (Sen slope, °C per decade) of T_{max}, T_{min}, T_{mid} and TR for 1981–2024 and 1981–2014.

Region	Var.	DJF 1981–2024	MAM 1981–2024	JJA 1981–2024	SON 1981–2024	DJF 1981–2014	MAM 1981–2014	JJA 1981–2014	SON 1981–2014
Dodoma	T_{max}	**−0.44**	**−0.78**	+0.05	+0.11	−0.22	**−0.60**	+0.23	**+0.26**
	T_{min}	**+0.20**	+0.09	+0.22	**+0.30**	+0.11	+0.11	+0.33	**+0.30**
	T_{mid}	−0.18	**−0.36**	+0.15	**+0.18**	−0.14	−0.27	**+0.28**	**+0.25**
	TR	**−0.66**	**−0.92**	**−0.20**	**−0.23**	−0.35	**−0.76**	−0.07	−0.05
Singida	T_{max}	−0.40	**−0.73**	−0.06	+0.05	−0.09	**−0.50**	+0.18	**+0.25**
	T_{min}	+0.16	+0.04	+0.17	**+0.23**	+0.10	+0.07	+0.27	+0.20
	T_{mid}	−0.14	**−0.34**	+0.07	+0.14	−0.00	−0.22	**+0.23**	**+0.26**
	TR	**−0.53**	**−0.81**	**−0.30**	**−0.28**	−0.12	**−0.62**	−0.03	−0.02
Tabora	T_{max}	−0.48	−0.72	−0.00	−0.01	**+0.34**	−0.09	**+0.33**	**+0.28**
	T_{min}	+0.11	+0.06	+0.02	+0.03	+0.08	+0.14	+0.40	**+0.21**
	T_{mid}	−0.19	−0.32	+0.01	+0.03	+0.21	+0.09	**+0.32**	**+0.24**
	TR	−0.52	**−0.76**	−0.21	−0.14	+0.12	−0.21	+0.07	+0.03

Note: trends computed on seasonal means with the modified Mann–Kendall test [33]; DJF series start in 1982. Values in bold are significant after Benjamini–Hochberg adjustment over the 48 tests of each period ($q < 0.05$) [35].

after the false-discovery-rate adjustment in nine of them: in all four seasons in Dodoma and Singida and in MAM in Tabora. The source of the narrowing depends on the season. In MAM it comes from $T_{\max}$, which fell by 0.78 and 0.73 °C per decade in Dodoma and Singida ($q < 0.001$) and by 0.72 °C per decade in Tabora ($q = 0.09$), while $T_{\min}$ showed no significant change; DJF $T_{\max}$ also fell in Dodoma (-0.44 °C per decade, $q < 0.001$). In SON, by contrast, the narrowing comes from $T_{\min}$, which rose by 0.30 °C per decade in Dodoma and 0.23 °C per decade in Singida ($q \leq 0.013$), while SON $T_{\max}$ showed no significant trend in any region.

Restricting the tests to 1981–2014, before the 2015–2016 step, reveals opposite seasonal tendencies that the annual means conceal, since annual $T_{\max}$ showed no significant trend over this period (Table 1). The dry season warmed: SON $T_{\max}$ rose in all three regions (0.25–0.28 °C per decade, $q \leq 0.013$), and T_{mid} rose in both JJA and SON in every region (0.23–0.32 °C per decade, $q \leq 0.041$). During the MAM rains the opposite occurred: $T_{\max}$ fell by 0.60 and 0.50 °C per decade in Dodoma and Singida ($q \leq 0.026$), and the MAM range narrowed in both regions ($q = 0.008$). Tabora differs in DJF, where $T_{\max}$ rose ($+0.34$ °C per decade, $q = 0.026$). The decline of $T_{\max}$ after 2015 is therefore not an isolated event in Dodoma and Singida: during the MAM rains it continues a decrease that was already under way before 2015. Whether these seasonal contrasts reflect changes in rainfall, cloud cover or soil moisture cannot be decided from temperature alone and requires additional variables.

3.2. Node degree of the temperature networks

Full-record graphs, using all 528 months of 1981–2024, were built for the T_{mid} series of each region. Fig. 5 draws them with a force-directed layout [38], in which strongly interconnected months are placed close together. Each network has 1936, 1933 and 1875 links in Dodoma, Singida and Tabora and forms an elongated chain whose order follows time: the rank correlation between the position of a month along the main axis of the layout and its date is 0.83–0.97. Most links are short — 90–92% join months no more than 12 months apart, and only 1.0–1.7% span more than five years. The chain is held together by a few large hubs, numbered in the figure, whose longest links reach 46–311 months (about 4–26 years) across the record.

In these networks, the average degree is 7.33, 7.33 and 7.10 in Dodoma, Singida and Tabora, but individual degrees range from 1 to 35, and the largest degree is 3.7–4.9 times the average (Fig. 6).

Table 4 ranks the five most connected months of each region. The leading hubs are December 1998 ($k = 32$), March 1988 ($k = 30$) and February 2006 ($k = 30$) in Dodoma; January 2006 ($k = 27$), December 1998 ($k = 26$) and November 2020 ($k = 26$) in Singida; and October 2017 ($k = 35$), October 1988 ($k = 30$) and December 1998 ($k = 28$) in Tabora. December 1998 is among the three most connected months in all three regions, and January–February 2006 is a leading hub in both Dodoma and Singida, which points to regional-scale rather than local forcing. Some hubs coincide with years of strong ENSO or IOD activity affecting East Africa, notably 1987–1988 and 1997–1999 [2, 3]; establishing a causal link, however, requires composite analysis against climate indices, which is beyond the scope of this paper.

Seasonal dependence. All hubs lie in the hot season between October and March, and this is a systematic property of the networks. The mean degree of each calendar month (Fig. 7a) is lowest in July (4.2–4.3) and highest in October–December (up to 9.9–

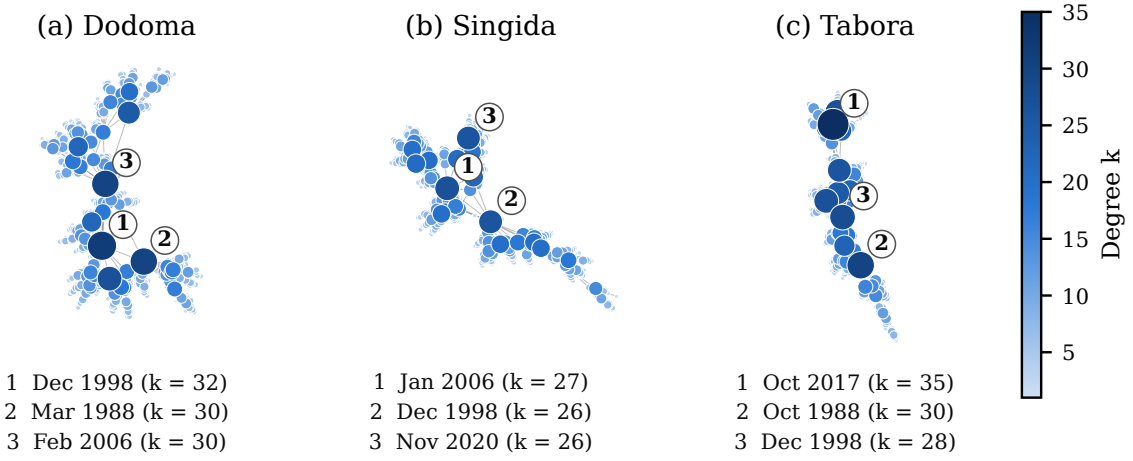

Figure 5: Full-record visibility graphs of the monthly T_{mid} series (528 months, 1981–2024) of (a) Dodoma, (b) Singida and (c) Tabora, drawn with the Fruchterman–Reingold force-directed layout. Node size and colour increase with degree k; the three highest-degree months of each network are numbered and listed below the panel.

Table 4: The five highest-degree months in the full-record T_{mid} network of each region.

Region	**Rank**	**Month**	T_{mid} **(°C)**	**Degree** k
Dodoma	1	Dec 1998	27.21	32
	2	Mar 1988	27.25	30
	3	Feb 2006	27.57	30
	4	Jan 1994	26.66	27
	5	Jan 2022	26.98	25
Singida	1	Jan 2006	24.84	27
	2	Dec 1998	25.07	26
	3	Nov 2020	23.38	26
	4	Oct 2023	24.25	22
	5	Nov 2013	24.23	21
Tabora	1	Oct 2017	26.34	35
	2	Oct 1988	26.57	30
	3	Dec 1998	27.03	28
	4	Oct 2004	26.23	27
	5	Nov 2019	24.97	27

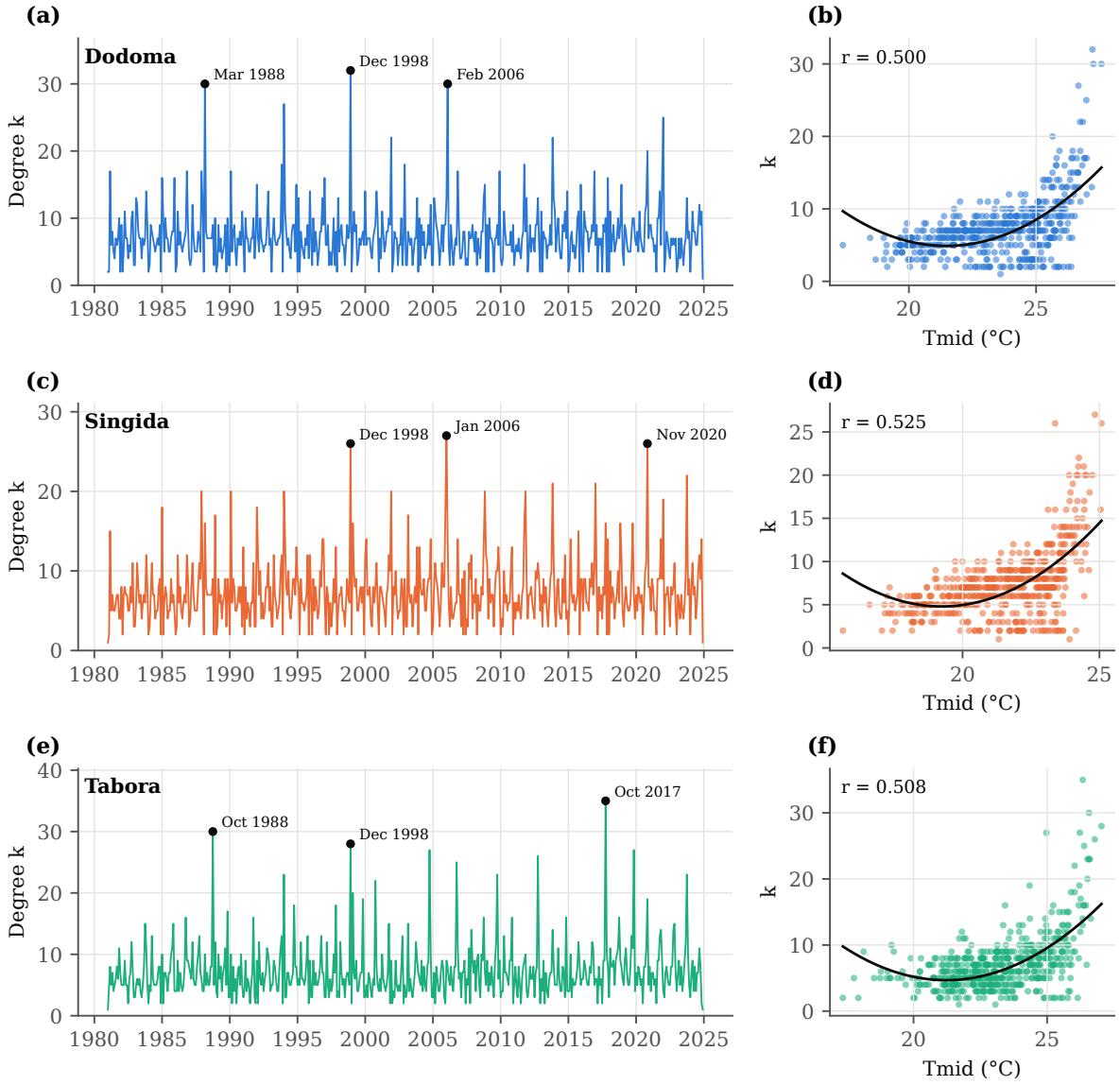

Figure 6: Degree structure of the full-record T_{mid} networks. (a), (c), (e) Degree of each month in Dodoma, Singida and Tabora, with the three highest-degree months marked. (b), (d), (f) Degree plotted against T_{mid}; black curves are quadratic fits and r is Pearson's correlation.

13.5), and every one of the 26 months with a degree in the top 5% falls in October–March in all three regions. The same pattern holds for $T_{\max}$, whose degrees are highest in October–November, while the $T_{\min}$ networks show a second maximum in April (Fig. 7b, c). Hot-season months stand above the cool-season trough and see across it to the hot seasons of other years, whereas mid-year months are hidden in the trough. A hub is therefore a hot-season month that also exceeds the hot seasons of the surrounding years.

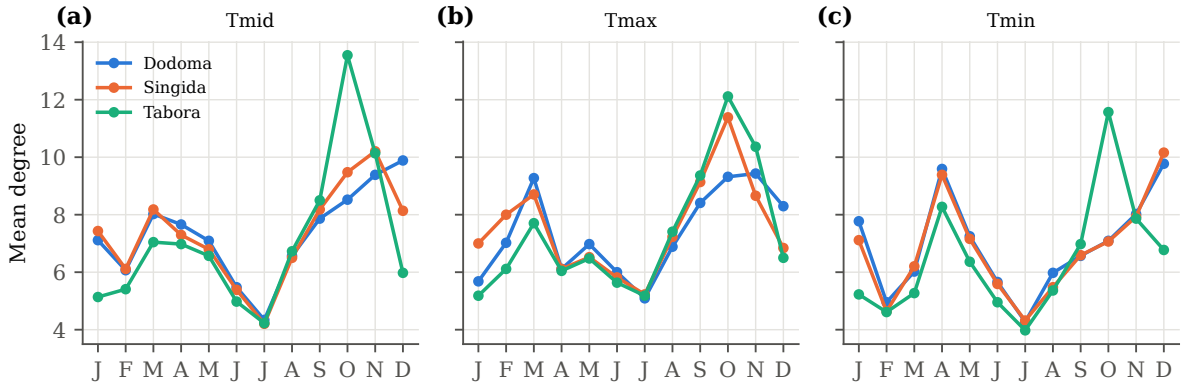

Figure 7: Mean degree of each calendar month in the full-record networks of (a) T_{mid}, (b) $T_{\max}$ and (c) $T_{\min}$.

Fig. 6(b, d, f) shows a clear positive association between temperature and degree ($r = 0.500$, 0.525 and 0.508; $p < 0.001$): the warmest months are generally the best connected, and cool-season months rarely become hubs. The association is not deterministic, however. In Singida, November 2020 (23.38 °C) is close to the average November (23.51 °C) yet ranks among the three most connected months ($k = 26$), because it occurred in the coolest year of the record (2020) and stands above the unusually cool hot seasons around it. Degree thus combines the level of a month with its contrast against neighbouring months.

Dependence on window length. Hub status could be an artefact of using the full 44-year record. Table 5 therefore follows the six leading Dodoma hubs through windows of 5–40 years, reporting for each hub the highest degree it reaches in any window that contains it.

Table 5: Highest degree reached by the leading Dodoma T_{mid} hubs in moving windows of W years.

Month	T_{mid} (°C)	Full record	W = 5	W = 10	W = 15	W = 20	W = 25	W = 30	W = 35	W = 40
Dec 1998	27.21	32	21	26	29	32	32	32	32	32
Mar 1988	27.25	30	18	25	28	29	29	30	30	30
Feb 2006	27.57	30	17	23	26	28	29	29	30	30
Jan 1994	26.66	27	20	26	27	27	27	27	27	27
Jan 2022	26.98	25	20	24	24	25	25	25	25	25
Dec 2001	26.84	22	19	22	22	22	22	22	22	22

In 5-year windows the hub degrees (17–21) lie well below their full-record values, because each hub can only see within its window. Degrees grow quickly with W, and from $W = 20$ years onwards December 1998 attains its full-record degree of 32. December 1998 has the highest degree for every window length (tied with January 1994 at $W = 10$),

so in Dodoma the leading hub does not depend on the length of the record. The same holds for October 2017 in Tabora, which leads at every window length. In Singida the order of the two leading hubs depends on the window: November 2020 has the highest degree for $W \leq 25$ years and January 2006 for $W \geq 30$ years, because the November 2020 maximum relies on the cool years immediately around it, whereas January 2006 overlooks a longer stretch of the record.

Table 6: Average Pearson correlation between T_{mid} and degree across moving windows.

Region	W = 5	W = 10	W = 15	W = 20	W = 25	W = 30	W = 35	W = 40
Dodoma	0.433	0.484	0.504	0.512	0.515	0.511	0.503	0.502
Singida	0.457	0.511	0.537	0.548	0.553	0.550	0.540	0.535
Tabora	0.519	0.525	0.538	0.536	0.537	0.536	0.523	0.503
Number of windows	40	35	30	25	20	15	10	5

Table 6 gives the average temperature–degree correlation across windows. The mean values stay between 0.433 and 0.553 for every region and window length, and individual windows range from 0.23 to 0.66. The positive association is therefore a feature of the whole record and not of any particular sub-period.

Dependence on temporal order. Fig. 8 repeats the scatter plots for reordered series. The positive relation remains and becomes stronger (mean r over 100 surrogates: 0.649 ± 0.014 in Dodoma, 0.643 ± 0.014 in Singida and 0.679 ± 0.015 in Tabora). In a shuffled series a warm value is usually surrounded by unrelated cooler values and can see far in both directions, so its degree depends almost entirely on its magnitude. In the observed series warm months cluster in the hot season, and neighbouring warm months block each other's view. The lower correlation in the real data is therefore a direct expression of the temporal organisation of temperature, and it confirms that the degree of a month carries information beyond its value.

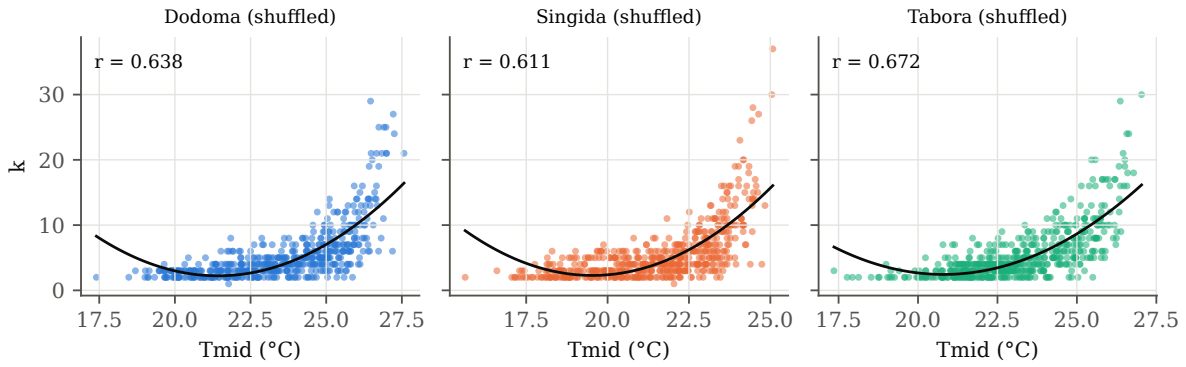

Figure 8: Degree versus T_{mid} after random reordering of the monthly values (one surrogate per region); black curves are quadratic fits.

3.3. Triadic motifs and their evolution

Over the full record, the motif composition of all three T_{mid} networks differs strongly from the white-noise reference (Fig. 9). The open peak motifs M_2 and M_4 occur far less often than in noise (M_2: 0.101–0.105; M_4: 0.105–0.148; noise: 0.199 and 0.200), whereas

the closed monotonic motifs M_7 and M_8 are roughly twice as common (M_7: 0.136–0.142; M_8: 0.109–0.128; noise: 0.064). M_7 and M_8 occur when temperature rises or falls along a convex path, so that the first and third months remain mutually visible. Their abundance is the micro-structural signature of the smooth annual cycle — the rise from August to November and the decline from December to July — in which successive months change gradually rather than at random.

To test for changes over time, the record was split at the end of 1999, the year after which annual $T_{\min}$ shifted upwards in Dodoma and Singida (Section 3.1). Motif frequencies were compared between the 109 windows of 120 months that end no later than December 1999 and the 181 windows that start after it (Fig. 9, Table 7).

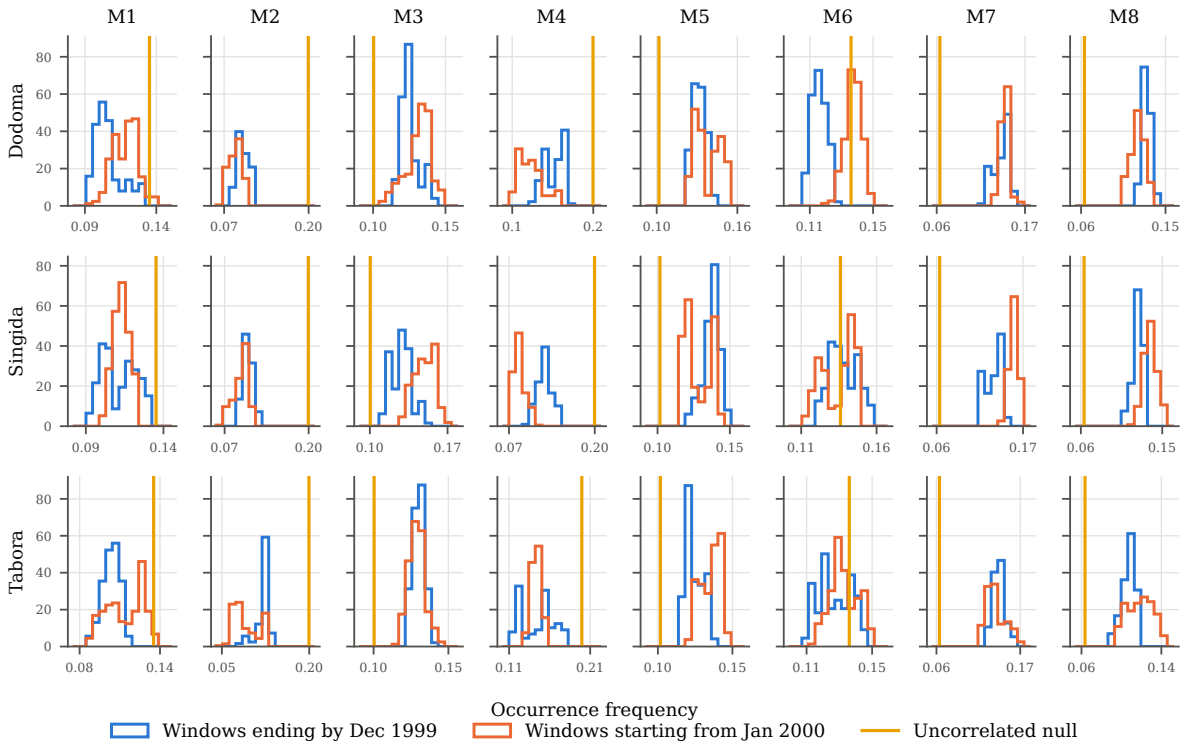

Figure 9: Frequency distributions of motifs M_1–M_8 across 120-month windows of the T_{mid} series, for windows ending by December 1999 (blue) and starting from January 2000 (orange); the yellow line marks the white-noise reference. Rows from top to bottom: Dodoma, Singida and Tabora.

The two groups of windows differ clearly. The open peak motif M_2 became less frequent in all three regions (0.099 → 0.087, 0.106 → 0.095 and 0.120 → 0.090), and M_4 declined sharply in Dodoma (0.152 → 0.123; $D = 0.73$) and Singida (0.123 → 0.086; $D = 0.98$). In Singida, the closed motifs M_3, M_7 and M_8 increased ($D = 0.76$, 0.95 and 0.76). Consequently, the share of closed triads rose in all three regions (0.527 → 0.534, 0.521 → 0.572 and 0.504 → 0.520). In short, after 1999 sharp single-month peaks became rarer and smoother, mutually visible sequences more common, in step with the upward shift in $T_{\min}$.

Fig. 10(a) traces the eight motif frequencies through time for Dodoma. On average M_7 and M_5 are the most frequent motifs and M_2 the least frequent; M_2 declines from about 0.105 in windows centred before 2000 to about 0.08 in windows centred in 2005–2010. M_4 is unusually frequent in windows centred around 1988–1993 and again after 2017. The

Table 7: Average motif frequencies in 120-month windows ending by December 1999 versus starting from January 2000 (T_{mid}), with the two-sample Kolmogorov–Smirnov distance D.

Motif	White noise	Dodoma	D	Singida	D	Tabora	D
M_1	0.135	0.106 → 0.119	0.60	0.111 → 0.113	0.38	0.104 → 0.114	0.50
M_2	0.199	0.099 → 0.087	0.43	0.106 → 0.095	0.38	0.120 → 0.090	0.67
M_3 (closed)	0.100	0.125 → 0.131	0.52	0.128 → 0.149	0.76	0.130 → 0.129	0.19
M_4	0.200	0.152 → 0.123	0.73	0.123 → 0.086	0.98	0.145 → 0.143	0.43
M_5 (closed)	0.102	0.132 → 0.138	0.43	0.138 → 0.128	0.49	0.124 → 0.135	0.57
M_6	0.136	0.116 → 0.137	0.97	0.138 → 0.134	0.26	0.127 → 0.133	0.33
M_7 (closed)	0.064	0.140 → 0.145	0.31	0.133 → 0.158	0.95	0.142 → 0.138	0.38
M_8 (closed)	0.064	0.130 → 0.120	0.59	0.123 → 0.137	0.76	0.107 → 0.118	0.51
Closed share	0.330	0.527 → 0.534	–	0.521 → 0.572	–	0.504 → 0.520	–

Note: successive windows overlap and are not independent, so Kolmogorov–Smirnov p-values overstate significance; D is reported as an effect size.

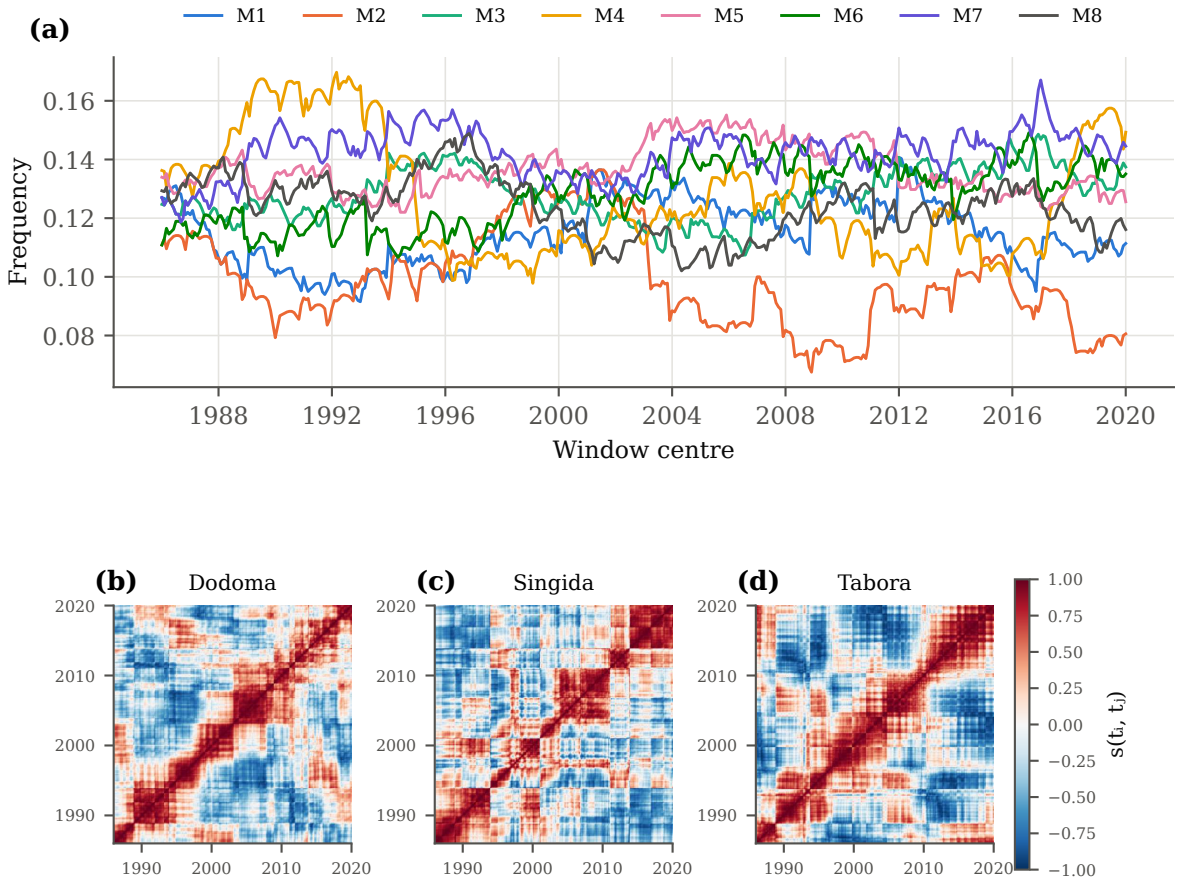

Figure 10: Evolution of motif composition. (a) Frequencies of M_1–M_8 in 120-month windows of the Dodoma T_{mid} series, plotted at window centres. (b)–(d) Pairwise correlation $s(t_i, t_j)$ between standardised motif vectors for Dodoma, Singida and Tabora.

similarity matrices of the standardised motif vectors (Fig. 10b–d) reveal distinct regimes. Windows centred before 1995 are strongly similar to one another (average $s = 0.41$–0.52), as are windows centred after 2012 (0.46–0.69), whereas the two periods are negatively related (-0.44–-0.16). Windows centred in 1997–2010 form a weaker, transitional block (0.24–0.39). The local organisation of temperature has therefore not been stationary, and its main reorganisation occurred around the turn of the century, consistent with the motif shift after 1999 and the $T_{\min}$ change points.

3.4. Degree distribution and persistence

Fig. 11 displays $P(k)$ on logarithmic axes and Table 8 lists the fitted parameters. Unlike the monotonic distributions expected for uncorrelated series, the distributions rise to a maximum at $k_{\mathrm{mode}} = 7$, 7 and 5 (Dodoma, Singida and Tabora): the annual cycle gives most months a moderate number of links. Beyond the mode, the tails follow Eq. (7) with $\gamma = 3.070$, 3.391 and 2.827 and adjusted R^2 of 0.898, 0.857 and 0.891, clearly better than an exponential decay (0.784, 0.777 and 0.778). The maximum-likelihood exponents (3.88, 3.77 and 2.87) are larger, which shows that exponents estimated from such short tails are uncertain, and fifteen-year sub-networks give $\gamma = 2.30$–3.49. Since a 528-node graph spans only about one decade of degree, these tails are best described as heavy-tailed and approximately scale-free rather than as strict power laws [26]. In practical terms, a small number of highly visible hot-season months stand out in the thermal history of each region, while the great majority of months exert only local influence; monitoring and early-warning efforts can therefore concentrate on recognising such months as they develop.

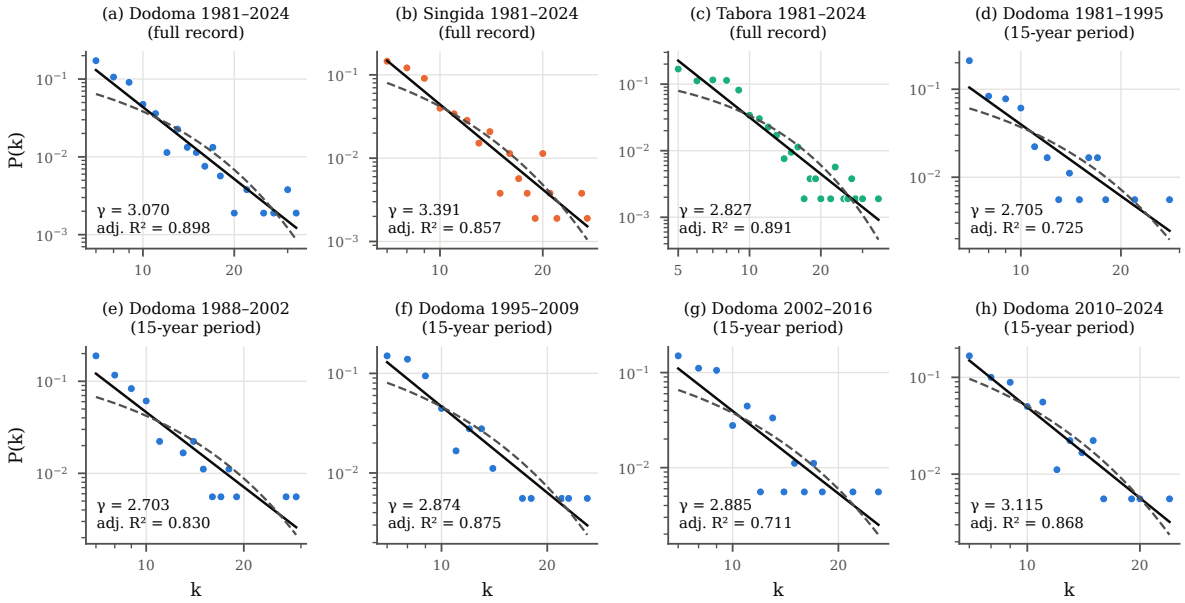

Figure 11: $P(k)$ on logarithmic axes for (a)–(c) the full-record T_{mid} networks of Dodoma, Singida and Tabora, each built from all 528 months of 1981–2024, and (d)–(h) Dodoma T_{mid} networks built separately for the 15-year periods 1981–1995, 1988–2002, 1995–2009, 2002–2016 and 2010–2024. Black lines are least-squares power-law fits and dashed grey lines exponential fits, both for $k \geq k_{\mathrm{mode}}$.

Table 8: Least-squares power-law parameters of the T_{mid} degree distributions (fitted for $k \geq k_{\mathrm{mode}}$) for the full record, 15-year sub-periods and shuffled surrogates.

Network	Dodoma γ	Adj. R^2	Exp. adj. R^2	Singida γ	Adj. R^2	Exp. adj. R^2	Tabora γ	Adj. R^2	Exp. adj. R^2
Full record (1981–2024)	3.070	0.898	0.784	3.391	0.857	0.777	2.827	0.891	0.778
Sub-period 1981–1995	2.705	0.725	0.563	3.204	0.829	0.780	2.314	0.916	0.775
Sub-period 1988–2002	2.703	0.830	0.656	3.185	0.907	0.859	2.468	0.928	0.884
Sub-period 1995–2009	2.874	0.875	0.763	3.494	0.847	0.776	2.396	0.820	0.693
Sub-period 2002–2016	2.885	0.711	0.579	2.872	0.895	0.888	2.411	0.794	0.709
Sub-period 2010–2024	3.115	0.868	0.789	2.970	0.876	0.776	2.297	0.744	0.545
Shuffled (mean of 100 runs)	2.204 ± 0.141	0.909	0.848	2.210 ± 0.136	0.908	0.849	2.257 ± 0.144	0.907	0.853

Note: "Exp. adj. R^2" is the adjusted R^2 of the alternative exponential model log P(k) = a − λk fitted over the same range.

Temporal order changes the degree distribution markedly. Shuffled series, which lack the annual cycle, have monotonically decreasing distributions with the most frequent degree at about 2–3 and flatter tails (γ = 2.20–2.26; Fig. 12a, Table 8). The seasonal cycle therefore raises the typical degree and steepens the tail, in line with the tendency of periodic signals to produce regular graphs [10], while the heavy tail itself reflects the interannual extremes superimposed on the cycle. Rescaled-range analysis (Fig. 12b) gives $H = 0.445$, 0.492 and 0.639 for Dodoma, Singida and Tabora, and the DFA exponents are 0.38, 0.40 and 0.61. In Dodoma and Singida the exponents lie below 0.5 and below the values obtained for shuffled series (H = 0.56–0.57, which include the known small-sample bias of the R/S estimator): within a few months the annual cycle returns temperature to its seasonal level, so fluctuations do not accumulate over long sub-series and the series behave as mean-reverting. Tabora is the exception ($H = 0.639$, $\alpha = 0.61$), because the prolonged cool period after 2017 adds a low-frequency component that both estimators interpret as persistence. Because both methods mix the seasonal oscillation with year-to-year variability, these exponents characterise the combined signal and should not be read as evidence of long-term memory.

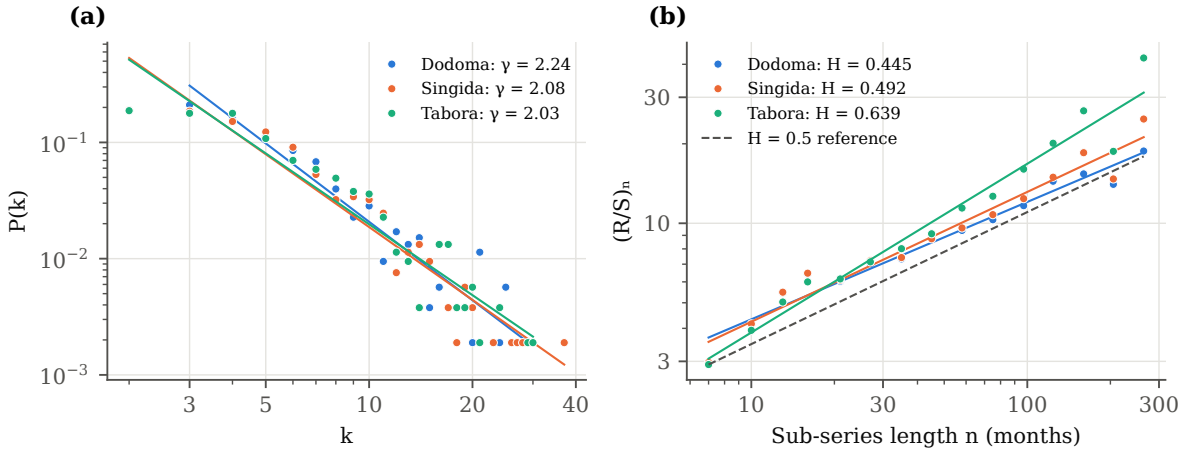

Figure 12: (a) $P(k)$ of networks built from shuffled T_{mid} series, with power-law fits for $k \geq k_{\mathrm{mode}}$. (b) Rescaled-range statistic of the observed T_{mid} series against sub-series length; the dashed line shows the slope expected without memory ($H = 0.5$).

Table 9: Network and persistence metrics for all nine temperature series.

Region	Var.	⟨k⟩	$k_{\max}$ (month)	r(T, k)	r shuffled	k_{mode}	γ	Adj. R^2	H (R/S)	DFA α
Dodoma	T_{mid}	7.33	32 (Dec 1998)	0.500	0.649	7	3.070	0.898	0.445	0.38
	$T_{\max}$	7.38	29 (Mar 1988)	0.465	0.660	6	2.960	0.888	0.495	0.44
	$T_{\min}$	6.91	30 (Dec 2017)	0.450	0.627	6	3.164	0.920	0.395	0.32
Singida	T_{mid}	7.33	27 (Jan 2006)	0.525	0.643	7	3.391	0.857	0.492	0.40
	$T_{\max}$	7.55	48 (Feb 1999)	0.481	0.652	6	2.677	0.852	0.565	0.49
	$T_{\min}$	6.80	33 (Dec 1987)	0.430	0.618	7	2.921	0.851	0.366	0.29
Tabora	T_{mid}	7.10	35 (Oct 2017)	0.508	0.679	5	2.827	0.891	0.639	0.61
	$T_{\max}$	7.34	30 (Feb 1999)	0.481	0.667	5	2.695	0.825	0.669	0.64
	$T_{\min}$	6.44	44 (Dec 1998)	0.455	0.601	5	2.637	0.835	0.492	0.43

Table 9 extends the analysis to $T_{\max}$ and $T_{\min}$. Each of the nine networks shows a positive temperature–degree correlation (0.430–0.525) that is weaker than in its shuffled counterpart (0.601–0.679), a peaked distribution with k_{mode} = 5–7 and a heavy tail (γ = 2.64–3.39; adjusted R^2 0.83–0.92). The most connected nodes of the study belong to the extremes: February 1999 in the Singida $T_{\max}$ network ($k = 48$), the hottest month of that record, and December 1998 in the Tabora $T_{\min}$ network ($k = 44$). The hot seasons of 1997–1998 and 1998–1999 thus stand out in all three regions: in each of the nine networks one of their months is among the six most connected nodes. The Hurst exponents of $T_{\min}$ (0.395, 0.366 and 0.492) are lower than those of $T_{\max}$ (0.495, 0.565 and 0.669), consistent with the larger share of the annual cycle in the variance of $T_{\min}$ (73–84%, against 47–59% for $T_{\max}$).

4. Conclusions

The monthly maximum and minimum temperatures of Dodoma, Singida and Tabora for 1981–2024, together with the mid-range temperature and the temperature range derived from them, were analysed with visibility graphs without removing the annual cycle. The main conclusions are as follows.

(1) A few months control the structure of each temperature network. December 1998 is among the three most connected months in all three regions, and in Dodoma it remains the most connected month for every window length from 5 to 40 years. All hubs and all months with the top 5% of degrees lie in the October–March hot season. Degree rises with temperature (r = 0.50–0.53) for all window lengths from 5 to 40 years, but less strongly than in shuffled data, so degree also reflects how sharply a month contrasts with its neighbours.

(2) The local ordering of successive months, described by triadic motifs, is rich in closed, monotonic triads generated by the smooth annual cycle. It changed after 1999: open peak motifs became rarer and the share of closed triads increased in all regions, in line with the upward shift in minimum temperature. Motif similarity matrices identify distinct regimes before and after the turn of the century.

(3) Degree distributions are peaked (k_{mode} = 5–7) with heavy, approximately power-law tails (γ = 2.83–3.39 for T_{mid}), whereas shuffled series give monotonic distributions with flatter tails. The annual cycle therefore organises the networks, and it also makes the series mean-reverting at the scales resolved by R/S and DFA in Dodoma and Singida.

(4) Between 1981 and 2014, the monthly minimum temperature warmed significantly in all three regions (0.18–0.24 °C per decade) while the monthly maximum showed no significant trend, so that the temperature range narrowed in Dodoma and Singida. After

2015–2016, the monthly maximum dropped abruptly by 1.0–2.4 °C in all regions; this step dominates the 1981–2024 trends, and its magnitude should be confirmed with station records.

(5) The seasonal analysis shows that the annual trends conceal opposite seasonal tendencies. Over 1981–2014, the dry season (June–November) warmed in all three regions, whereas maximum temperature fell during the March–May rains in Dodoma and Singida. Over 1981–2024, the temperature range narrowed in nine of the twelve region–season combinations, through falling maximum temperature in the rainy season and, in Dodoma and Singida, rising minimum temperature in September–November.

These results show that network measures reveal aspects of temperature variability — the prominence and seasonal timing of individual months, the arrangement of successive months and changes of regime — that trend analysis alone does not capture. Natural next steps are to repeat the analysis with daily data, to relate the hubs and regimes to ENSO, IOD and rainfall indices, and to couple temperature and rainfall through multiplex visibility graphs.

CRediT authorship contribution statement

Shaban Juma Ally: Conceptualization, Methodology, Formal analysis, Data curation, Validation, Writing – review and editing, Writing – original draft.
Begari Muniswamy: Conceptualization, Supervision, Writing – review and editing.
B. Punyavathi: Data curation.

Declaration of competing interest

The authors declare that they have no known competing financial interests.

Funding

This research did not receive any specific grant from funding agencies in the public, commercial, or not-for-profit sectors.

Data availability

The monthly temperature data (1981–2024) were obtained from the NASA POWER project and are publicly available at https://power.larc.nasa.gov/.

Declaration of generative AI and AI-assisted technologies in the manuscript preparation process

AI was used solely for language improvement in the manuscript. After using this tool, the authors reviewed and edited the content as needed and take full responsibility for the content of the published article.

Acknowledgements

The authors gratefully acknowledge Andhra University and the College of African Wildlife Management for providing a conducive academic and research environment that supported the successful completion of this study.

References

[1] IPCC. Climate change 2021: The physical science basis. Contribution of Working Group I to the Sixth Assessment Report of the Intergovernmental Panel on Climate Change. Masson-Delmotte V, et al., editors. Cambridge: Cambridge University Press; 2021. https://doi.org/10.1017/9781009157896.

[2] Nicholson SE. Climate and climatic variability of rainfall over eastern Africa. Rev Geophys 2017;55:590-635. https://doi.org/10.1002/2016RG000544.

[3] Saji NH, Goswami BN, Vinayachandran PN, Yamagata T. A dipole mode in the tropical Indian Ocean. Nature 1999;401:360-3. https://doi.org/10.1038/43854.

[4] Luhunga PM, Kijazi AL, Chang'a L, Kondowe A, Ng'ongolo H, Mtongori H. Climate change projections for Tanzania based on high-resolution regional climate models from the Coordinated Regional Climate Downscaling Experiment (CORDEX)-Africa. Front Environ Sci 2018;6:122. https://doi.org/10.3389/fenvs.2018.00122.

[5] Magang DS, Ojara MA, Lou Y, King'uza PH. Future climate projection across Tanzania under CMIP6 with high-resolution regional climate model. Sci Rep 2024;14:12741. https://doi.org/10.1038/s41598-024-63495-w.

[6] Myeya HE. Recent temperature and rainfall characteristics in Dodoma Region, central Tanzania (1961–2013). Ghana J Geogr 2021;13:63-80. https://doi.org/10.4314/gjg.v13i1.4.

[7] Msilu S, Majule AE, Perfect J. Analysis of rainfall and temperature dynamics (1981 to 2021) in semi-arid central Tanzania. Ghana J Geogr 2024;16:84-94. https://doi.org/10.4314/gjg.v16i2.9.

[8] Zhang J, Small M. Complex network from pseudoperiodic time series: Topology versus dynamics. Phys Rev Lett 2006;96:238701. https://doi.org/10.1103/PhysRevLett.96.238701.

[9] Marwan N, Donges JF, Zou Y, Donner RV, Kurths J. Complex network approach for recurrence analysis of time series. Phys Lett A 2009;373:4246-54. https://doi.org/10.1016/j.physleta.2009.09.042.

[10] Lacasa L, Luque B, Ballesteros F, Luque J, Nuño JC. From time series to complex networks: The visibility graph. Proc Natl Acad Sci USA 2008;105:4972-5. https://doi.org/10.1073/pnas.0709247105.

[11] Luque B, Lacasa L, Ballesteros F, Luque J. Horizontal visibility graphs: Exact results for random time series. Phys Rev E 2009;80:046103. https://doi.org/10.1103/PhysRevE.80.046103.

[12] Lacasa L, Luque B, Luque J, Nuño JC. The visibility graph: A new method for estimating the Hurst exponent of fractional Brownian motion. EPL 2009;86:30001. https://doi.org/10.1209/0295-5075/86/30001.

[13] Ni X-H, Jiang Z-Q, Zhou W-X. Degree distributions of the visibility graphs mapped from fractional Brownian motions and multifractal random walks. Phys Lett A 2009;373:3822-6. https://doi.org/10.1016/j.physleta.2009.08.041.

[14] Iacovacci J, Lacasa L. Sequential visibility-graph motifs. Phys Rev E 2016;93:042309. https://doi.org/10.1103/PhysRevE.93.042309.

[15] Iacovacci J, Lacasa L. Sequential motif profile of natural visibility graphs. Phys Rev E 2016;94:052309. https://doi.org/10.1103/PhysRevE.94.052309.

[16] Xie W-J, Han R-Q, Zhou W-X. Tetradic motif profiles of horizontal visibility graphs. Commun Nonlinear Sci Numer Simul 2019;72:544-51. https://doi.org/10.1016/j.cnsns.2019.01.012.

[17] Donges JF, Zou Y, Marwan N, Kurths J. Complex networks in climate dynamics: Comparing linear and nonlinear network construction methods. Eur Phys J Spec Top 2009;174:157-79. https://doi.org/10.1140/epjst/e2009-01098-2.

[18] Tsonis AA, Swanson KL. Topology and predictability of El Niño and La Niña networks. Phys Rev Lett 2008;100:228502. https://doi.org/10.1103/PhysRevLett.100.228502.

[19] Elsner JB, Jagger TH, Fogarty EA. Visibility network of United States hurricanes. Geophys Res Lett 2009;36:L16702. https://doi.org/10.1029/2009GL039129.

[20] Rosales-Pérez JA, Canto-Lugo E, Valdés-Lozano D, Huerta-Quintanilla R. Temperature time series analysis at Yucatan using natural and horizontal visibility algorithms. PLoS One 2019;14:e0226598. https://doi.org/10.1371/journal.pone.0226598.

[21] Gómez-Gómez J, Carmona-Cabezas R, Sánchez-López E, Gutiérrez de Ravé E, Jiménez-Hornero FJ. Analysis of air mean temperature anomalies by using horizontal visibility graphs. Entropy 2021;23:207. https://doi.org/10.3390/e23020207.

[22] Zhang P, Ning P, Cao R, Xu J. Analysis of climate change characteristics in Xi'an based on the visibility graph. Front Phys 2021;9:702064. https://doi.org/10.3389/fphy.2021.702064.

[23] Cao R-H, Deng Z-H, Xu J-W. Analysis of precipitation characteristics in Shanghai based on the visibility graph algorithm. Physica A 2022;597:127227. https://doi.org/10.1016/j.physa.2022.127227.

[24] [dataset] NASA Langley Research Center. Prediction of Worldwide Energy Resources (POWER) Project, https://power.larc.nasa.gov/; n.d. [accessed 23 November 2026].

[25] Milo R, Shen-Orr S, Itzkovitz S, Kashtan N, Chklovskii D, Alon U. Network motifs: Simple building blocks of complex networks. Science 2002;298:824-7. https://doi.org/10.1126/science.298.5594.824.

[26] Clauset A, Shalizi CR, Newman MEJ. Power-law distributions in empirical data. SIAM Rev 2009;51:661-703. https://doi.org/10.1137/070710111.

[27] Barabási A-L, Albert R. Emergence of scaling in random networks. Science 1999;286:509-12. https://doi.org/10.1126/science.286.5439.509.

[28] Hurst HE. Long-term storage capacity of reservoirs. Trans Am Soc Civ Eng 1951;116:770-99. https://doi.org/10.1061/TACEAT.0006518.

[29] Peng C-K, Buldyrev SV, Havlin S, Simons M, Stanley HE, Goldberger AL. Mosaic organization of DNA nucleotides. Phys Rev E 1994;49:1685-9. https://doi.org/10.1103/PhysRevE.49.1685.

[30] Easterling DR, Horton B, Jones PD, Peterson TC, Karl TR, Parker DE, et al. Maximum and minimum temperature trends for the globe. Science 1997;277:364-7. https://doi.org/10.1126/science.277.5324.364.

[31] Mann HB. Nonparametric tests against trend. Econometrica 1945;13:245-59. https://doi.org/10.2307/1907187.

[32] Kendall MG. Rank correlation methods. 4th ed. London: Charles Griffin; 1975.

[33] Hamed KH, Rao AR. A modified Mann–Kendall trend test for autocorrelated data. J Hydrol 1998;204:182-96. https://doi.org/10.1016/S0022-1694(97)00125-X.

[34] Sen PK. Estimates of the regression coefficient based on Kendall's tau. J Am Stat Assoc 1968;63:1379-89. https://doi.org/10.1080/01621459.1968.10480934.

[35] Benjamini Y, Hochberg Y. Controlling the false discovery rate: A practical and powerful approach to multiple testing. J R Stat Soc Ser B Methodol 1995;57:289-300. https://doi.org/10.1111/j.2517-6161.1995.tb02031.x.

[36] Pettitt AN. A non-parametric approach to the change-point problem. J R Stat Soc Ser C Appl Stat 1979;28:126-35. https://doi.org/10.2307/2346729.

[37] Gelaro R, McCarty W, Suárez MJ, Todling R, Molod A, Takacs L, et al. The Modern-Era Retrospective Analysis for Research and Applications, Version 2 (MERRA-2). J Clim 2017;30:5419-54. https://doi.org/10.1175/JCLI-D-16-0758.1.

[38] Fruchterman TMJ, Reingold EM. Graph drawing by force-directed placement. Softw Pract Exp 1991;21:1129-64. https://doi.org/10.1002/spe.4380211102.